Effects of Magnet Errors in the ILC 14 mrad Extraction Line[*]

Dragan Toprek
VINCA Institute of Nuclear Sciences, 11001 Belgrade, Serbia[††]
The Cockcroft Institute, University of Manchester, UK[‡‡]

Yuri Nosochkov
SLAC National Accelerator Laboratory, 2575 Sand Hill Road, Menlo Park, CA 94025, USA

Abstract

The ILC baseline extraction line is designed for 14 mrad horizontal crossing angle between e+ and e- colliding beams at Interaction Point (IP). The extraction optics in the Interaction Region (IR) includes a detector integrated dipole field (anti-DID) to reduce orbit perturbation caused by the detector solenoid and minimize detector background. This paper presents a study of random field and alignment errors in the extraction magnets, compensation of the induced orbit perturbation, and effects of errors on extraction beam power loss. The results are obtained for the baseline ILC energy of 500 GeV center-of-mass and three options of beam parameters.

Effects of Magnet Errors in the ILC 14 mrad Extraction Line[§§]

Dragan Toprek
VINCA Institute of Nuclear Sciences, 11001 Belgrade, Serbia[***]
The Cockcroft Institute, University of Manchester, UK[†††]

Yuri Nosochkov
SLAC National Accelerator Laboratory, Menlo Park, CA 94025, USA

The ILC baseline extraction line is designed for 14 mrad horizontal crossing angle between e+ and e- colliding beams at Interaction Point (IP). The extraction optics in the Interaction Region (IR) includes a detector integrated dipole field (anti-DID) to reduce orbit perturbation caused by the detector solenoid and minimize detector background. This paper presents a study of random field and alignment errors in the extraction magnets, compensation of the induced orbit perturbation, and effects of errors on extraction beam power loss. The results are obtained for the baseline ILC energy of 500 GeV center-of-mass and three options of beam parameters.

1. INTRODUCTION

The ILC baseline extraction line is designed for 14 mrad horizontal crossing angle between e+ and e− colliding beams at Interaction Point (IP) [1]. The extraction optics provides large beam acceptance in order to minimize beam losses caused by large angular spread and long energy tail in the disrupted primary and secondary beams. It also includes dedicated vertical chicanes for beam energy measurement and gamma calorimeter (GAMCAL) diagnostics, and a low β focal point with 2 cm vertical dispersion used as a Compton Interaction Point (CIP) for polarization measurement.

The crossing angle scheme naturally results in a horizontal angle between beam trajectory and direction of the detector solenoid field B_s, equal to half-crossing angle $\theta_c = 7$ mrad. This angle creates a systematic horizontal field component $B_x = B_s \sin\theta_c$ on the beam trajectory which causes vertical beam deflection and therefore produces vertical orbit and dispersion, synchrotron radiation and rotation of beam polarization vector. In addition, the solenoid field creates a weak focusing effect in *x-y* planes and coupling of *x-y* betatron motion which alter the downstream beam properties. Perturbation of the extracted beam caused by the solenoid needs to be compensated in order to avoid a higher beam loss and preserve the desired beam properties at the Compton IP for polarization measurement. The incoming and extraction optics share a detector integrated dipole field (anti-DID) near the IP in order to reduce the amplitude of the extraction particle trajectories induced by the solenoid and therefore minimize the detector background.

This paper presents calculations of the effects of random field and alignment errors in the extraction magnets with and without their correction, using MAD [2] and DIMAD [3] codes. It is assumed that the incoming beam at IP has the design parameters except an uncorrected 50 μrad vertical orbit angle generated by the upstream part of the solenoid and anti-DID. The calculations are done for the push-pull version of the extraction optics [4,5] with the final focus drift of

---

[***] Author's present address.
[†††] Author's affiliation when this study began.

L^* = 3.51 m and the SiD [6,7] detector solenoid field model, for the nominal ILC energy of 500 GeV center-of-mass (CM) and three options of beam parameters.

1.1. Extraction Line Optics

Beam optics of the 14 mrad extraction line and three options of ILC beam parameters are described in Refs. [4,8]. Length of the extraction line from IP to dump is about 300 m. The first superconducting (SC) *incoming* quadrupole QD0 is located at distance of L^* = 3.51 m from IP, and the first *extraction* SC quadrupole QDEX1 is at 5.5 m to provide sufficient horizontal separation from the incoming line. These two quadrupoles and the incoming sextupole SD0 will be part of a detector in a push-pull configuration [5]. Beam apertures of the extraction SC quadrupoles QDEX1 and QFEX2A are set to the maximum values of R = 15 mm and 30 mm, respectively, limited by the separation from the incoming magnets. The remaining downstream extraction quadrupoles are warm magnets starting at distance of 17.19 m from IP. The extraction quadrupole system is designed to provide: 1) a low β focal point at 148.6 m from IP, where the Compton IP will be located, 2) the optimal transformation term R_{22} = −0.5 from IP to CIP for efficient polarization measurement, and 3) large chromatic and geometric acceptance for keeping the disrupted beam loss at acceptable level. Downstream of the quadrupoles, the extraction line includes a four bend vertical chicane for measurements of beam energy, a four bend vertical chicane for polarization measurement, and two vertical bends for gamma calorimeter luminosity diagnostics [9]. The polarimeter bends create 2 cm vertical dispersion at the Compton IP located at center of the polarimeter chicane. After the last GAMCAL bend magnet, the extraction line contains a set of 5 horizontal and 5 vertical fast kickers, located on average ~85 m before the dump. The rapidly oscillating kicker field (~1 kHz) will sweep the beam along a R = 3 cm circle at the dump in order to increase the effective beam area for protecting the dump window from high power density of small undisrupted beam and preventing water boiling in the dump vessel.

The extraction collimation system includes two collimators in the chicanes. The first one is placed at center of the energy chicane, 60.7 m after IP, where momentum dispersion is 17 mm. Its 40 mm vertical aperture on the low energy side of the beam is set to remove the low energy tail electrons with relative energies below 30-35%. The second collimator at 160.9 m is inside the polarimeter chicane to protect the Cherenkov detector (at 175.6 m) from synchrotron radiation created in the energy chicane bends. Three more collimators (COLW1, COLW2 and COLW3) are included in the final 100 m section before the dump in order to protect the fast sweeping kickers and limit beam size to within R = 15 cm at the dump window.

1.2. Parameter Options and Disrupted Beam Properties at IP

Distributions of primary disrupted beams at IP were generated using GUINEA-PIG beam-beam simulation code [10]. Beam disruption in collision creates a very long tail of low energy particles and large angular divergence in the outgoing beams. Three beam parameter options were studied [11,12]: 1) nominal (C11), 2) with a large vertical emittance (C13), and 3) with a low beam power (C14). These parameter settings are based on different values of emittance, beam current and beam size at IP, but they provide the same design luminosity. Consequently, the effect of beam disruption varies in these options. The low power option C14 yields the strongest disruption effect leading to a larger extracted beam. The disruption can be further enhanced by a vertical offset between the e+ and e- beams at IP. Therefore, for each parameter option two cases were studied: without a vertical offset and with a vertical offset

corresponding to maximum disruption effect. The selected full beam-to-beam vertical offsets Δy in the C11, C13, C14 options are 200 nm, 300 nm, and 120 nm, respectively. Note that in the machine operation any IP offsets will be actively compensated to minimize their effects on luminosity and beam disruption. A horizontal beam offset is not studied in this paper since it reduces the disruption effect for flat beams [13] and therefore is not a concern for extracted beam. Beam parameters used in this study are listed in Table 1 [11].

Table 1: Beam parameters at IP for 500 GeV CM energy.

Parameter	Nominal C11	Large Y-Emit C13	Low Power C14
Number of particles per bunch, N	$2 \cdot 10^{10}$	$2 \cdot 10^{10}$	$2 \cdot 10^{10}$
Number of bunches per train, N_b	2820	2820	1330
Repetition frequency, f [Hz]	5	5	5
Norm. emittance, $\gamma \varepsilon_x$ [$m \cdot rad$]	$1 \cdot 10^{-5}$	$1.2 \cdot 10^{-5}$	$1 \cdot 10^{-5}$
Norm. emittance, $\gamma \varepsilon_y$ [$m \cdot rad$]	$4 \cdot 10^{-8}$	$8 \cdot 10^{-8}$	$3.5 \cdot 10^{-8}$
Beta function, β_x^* [mm]	21	10	10
Beta function, β_y^* [mm]	0.4	0.4	0.2
RMS beam size, σ_x^* [nm]	655	495	452
RMS beam size, σ_y^* [nm]	5.7	8.1	3.8
RMS bunch length, σ_z^* [μm]	300	500	200
Energy loss by beamstrahlung, δ_{BS}	0.022	0.024	0.057
Beam power, P [MW]	11.3	11.3	5.3
Luminosity, $\mathcal{L}$ [$cm^{-2}s^{-1}$]	$2 \cdot 10^{34}$	$2 \cdot 10^{34}$	$2 \cdot 10^{34}$

Tracking of $\sim 10^5$ particles is typically sufficient for adequate simulation of beam distribution in the extraction line and for calculation of relatively high beam loss in collimators. However, accurate estimate of much lower losses in magnets typically requires a much higher statistics of $>10^7$ particles in the simulated beam. The latter, unfortunately, significantly increases the simulation running time and requires large computer storage space. Fortunately, for the purpose of beam loss calculation in magnets, it is not necessary to track a full beam because only very low energy particles are lost in extraction magnets due to over-focusing and dispersion. In this case, it is sufficient to track only the lowest part of beam energy tail and particles with large initial x-y angles. As a result, two types of particle data files were used in this study. The low statistics files containing total of $\sim 7 \cdot 10^4$ particles in two beams were used for evaluation of beam distribution and polarization at Compton IP, and for calculation of high beam loss in extraction collimators. The high statistics files with total of up to $3.5 \cdot 10^7$ particles in two beams were generated for the purpose of beam loss calculation in extraction magnets. But for tracking simulations, these files were reduced to much smaller files containing $\leq 10^5$ particles with relative energies below 65% and/or initial x-y angles larger than ± 0.5 mrad. For maximum statistics, the above files contain both e+ and e− colliding beam distributions, but assuming the same charge

for all particles. In case of ideal collisions without beam offset at IP, the e+ and e− disrupted distributions are identical, therefore combining the two beams does not make difference. In case of a non-zero IP vertical offset, the outgoing e+ and e- beams will have the same but opposite systematic offsets of y and y' at IP. In this case, combining e+ and e− beams is equivalent to combining two beams with initial positive and negative vertical offsets. Therefore, the resultant power loss will be an average of power losses with positive and negative offsets at IP.

The disrupted beam distributions at IP, obtained by GUINEA-PIG, for the three beam parameter options without and with vertical offset are shown in Ref. [8] in Figures 4-9, and distributions of particle energies are presented in Fig. 10 in the same Reference.

Fig. 1 shows the disrupted β functions and dispersion in the 14 mrad extraction line without magnet errors, as calculated by MAD, for the Nominal parameter option C11 in presence of the detector solenoid field, the anti-DID field and orbit correction in the solenoid and polarimeter chicane regions. The incoming vertical orbit angle at IP is assumed to be 50 µrad. Beta functions are focused by the extraction quadrupoles to a low β waist at the Compton IP ($s = 148.6$ m) with the transformation matrix term $R_{22} = -0.5$ from IP to CIP, suitable for polarization measurements. The orbit caused by the post-IP detector solenoid, anti-DID field and 50 µrad IP y-angle is canceled locally in the solenoid and polarimeter regions as shown Fig. 2. At the Compton IP the local polarimeter correctors are set to make the same orbit angle as at the IP, i.e. $y'(CIP) = 50$ µrad and $x'(CIP) = 0$. Although the local solenoid correctors are not specifically designed to compensate the solenoid dispersion, they provide almost complete correction as shown in Fig. 1, because their positions are close to the solenoid. This compensation should be sufficient for polarization measurement.
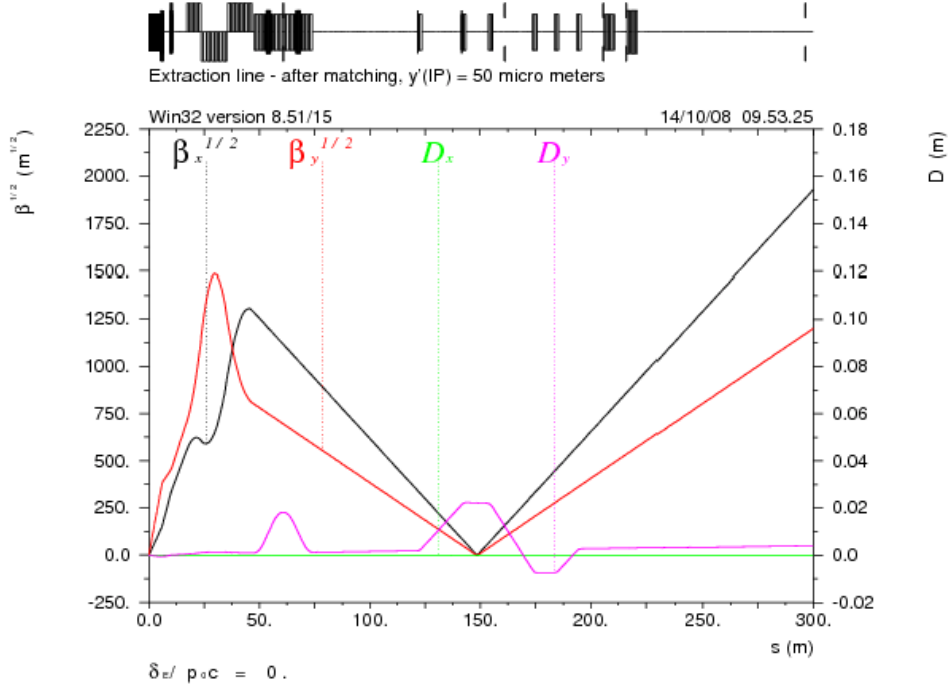
Figure 1: Disrupted β functions and dispersion in the 14 mrad extraction line for the Nominal parameter option. The IP vertical orbit angle is $y'(IP) = 50$ µrad, and the Compton IP angle is corrected to $y'(CIP) = 50$ µrad.

The solenoid weak focusing creates a shift of the low beta waist away from Compton IP resulting in a larger beam size at the CIP. This effect can be compensated by using two quadrupole corrector coils on the extraction quadrupoles. These correctors can be used to maintain the point-to-point focusing from IP to CIP by adjusting the transfer matrix terms R_{12} and R_{34} to zero. Previous studies did not find a significant effect of solenoid coupling on the extraction beam properties; therefore no coupling correction has been considered.
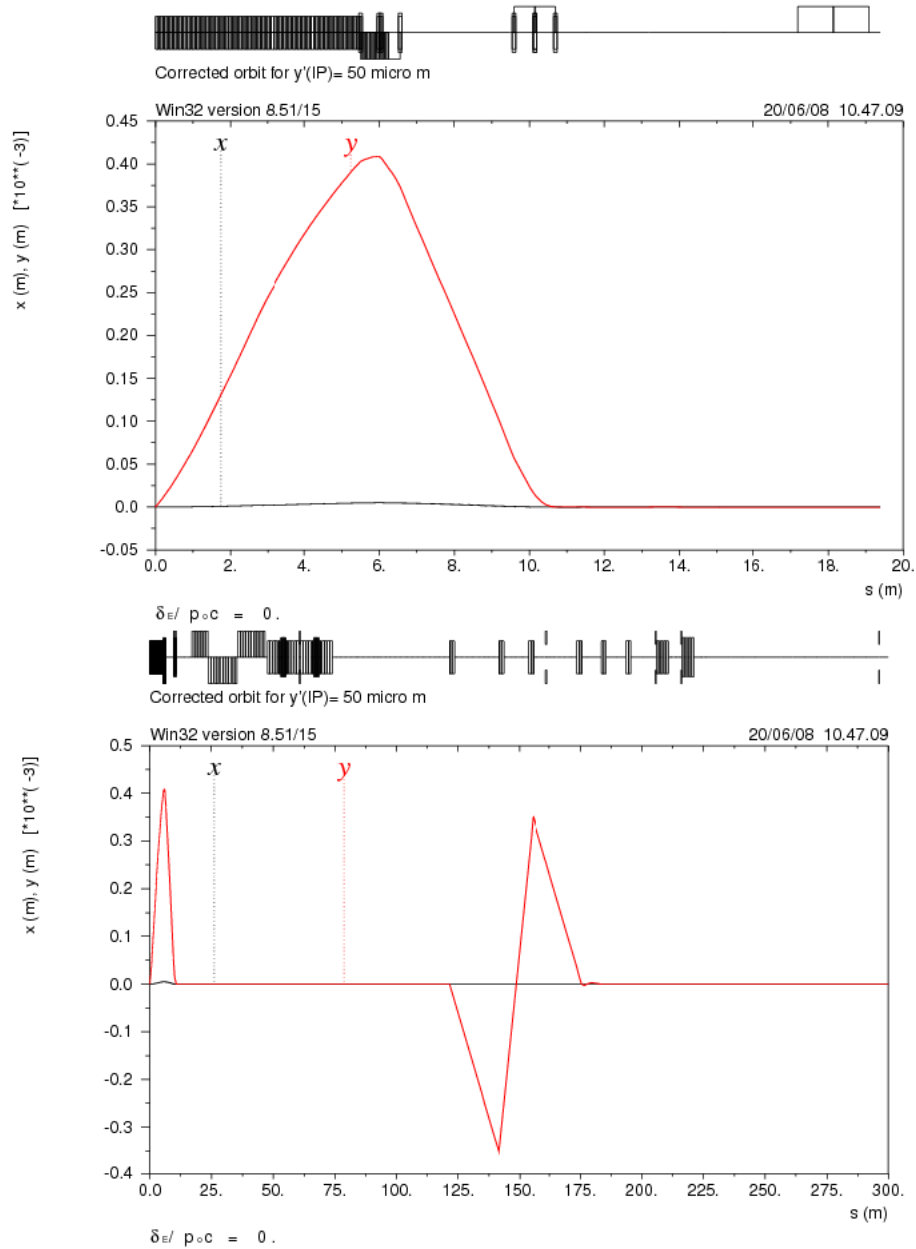
Figure 2: Corrected *X* and *Y* orbit in the 14 mrad extraction line. The top figure shows the first 20 m after IP. The IP vertical orbit angle is *y´*(*IP*) = 50 µrad, and the Compton IP angle is corrected to *y´*(C*IP*) = 50 µrad.

5

2. BEAM POWER LOSS WITHOUT MAGNET ERRORS

The primary disrupted beam power losses were calculated using DIMAD tracking. As described earlier, two types of particle data files were used. The relatively low statistics files with $\sim 7 \cdot 10^4$ particles for combined beams were used to calculate the relatively large losses on extraction collimators. The high statistics files based on $3.5 \cdot 10^7$ particles in the combined beams were used to estimate low losses in the extraction magnets. Since it is known that only particles with the lowest energies and largest IP angles are lost in the magnets, the high statistics files were reduced to much smaller files containing only beam tails where the relative particle energies are below 65% and/or their IP angles exceed 0.5 mrad. In this tracking, the solenoid, the anti-DID and the compensating dipole correctors are turned on, and the vertical orbit at Compton IP is adjusted to have the same angle as at IP, i.e. $y'(CIP) = y'(IP) = 50$ µrad.

The tracking found no power losses in the extraction quadrupoles for the Nominal and Low Y-emittance parameter options. Therefore only the results for the Low Power option are presented in Table 2. Note that no primary loss was observed in the sensitive SC quadrupoles, and the maximum loss in warm quadrupoles is 1.4 W for collisions without IP offset and 25 W for collisions with IP *y*-offset. This loss level is acceptable and should not cause long-term radiation damage. Note that the large beam offsets at IP will be actively corrected in real beam operation in order to maintain high luminosity, therefore the high beam loss caused by the IP offsets will be limited to short periods of time and therefore on average will be significantly lower.

In Table 2 the numbers shown in black colour correspond to the case when the field and alignment errors are NOT applied. The meaning of the other colours (red and green) will be explained later (see Section 4). The columns "BEFORE CORRECTIONS" and "AFTER CORRECTIONS" in Table 2 correspond to the cases with errors before and after correction, respectively. The description of errors and their type will be also explained in Section 4.

Power losses in the extraction collimators, in the case when the field and alignment errors are not applied, are summarized in Table 3 for the three parameter options without and with IP offset. In this tracking, the fast sweeping kickers were set to sweep the beam on $R = 3$ cm circle at dump. Under ideal IP conditions without beam offset, the maximum power loss in a single collimator is near 21 kW. With the large *y*-offset, the maximum collimator loss can be up to 64 kW. However, as mentioned earlier, the IP offsets will be actively corrected and therefore the average loss will be lower. Most of the high loss occurs in the final three collimators COLW1,2,3 which purpose is to clean-up the beam tails before the dump. Since there are no magnets or diagnostic in most of this region, this high loss is not of a significant concern. The clean-up collimator COLE and protection collimator COLCD are located in the energy and polarimeter chicanes where the beam loss is much lower.

Table 2: Primary disrupted beam loss (W) in the extraction quadrupoles for the Low Power parameter option without and with IP *y*-offset for the selected magnet errors. Black colour – errors are not applied, green – bend magnet field errors (in brackets – bend magnet misalignment), red – quad field errors (in brackets – quad misalignment), blue – detector solenoid field error (in brackets – solenoid misalignment).

Quadrupole	BEFORE CORRECTIONS		AFTER CORRECTIONS	
	C14	C14, y-offset	C14	C14, y-offset
QDEX1 (SC)	0	0	0	0
QFEX2A (SC)	0	0	0	0
QFEX2B	0	0	0	0
QFEX2C	0	0	0	0
QFEX2D	0	0	0	0
QDEX3A	0	0.3	0	0.3
	0 (0)	0.7 (0.7)	0 (0)	0.7 (0.7)
	0 (0)	0.7 (0.7)	0 (0)	0.7 (0.7)
	0 (0)	0.7 (0.7)	0 (0)	0.9 (0.9)
QDEX3B	0	0	0	0
	0 (0)	0 (0)	0 (0)	0 (0)
	0 (0)	0 (0.2)	0 (0)	0 (0.2)
	0 (0)	0 (0)	0 (0)	0 (0.1)
QDEX3C	0.1	0	0.1	0
	0.2 (0.2)	0 (0)	0.2 (0.2)	0 (0)
	0.2 (0.2)	0 (0)	0.2 (0.2)	0 (0)
	0.2 (0.2)	0 (0)	0.2 (0.2)	0 (0)
QDEX3D	0.5	0	0.5	0
	1.1 (1.1)	0 (0)	1.0 (1.0)	0 (0)
	1.1 (1.3)	0 (0)	1.0 (1.0)	0 (0)
	1.1 (1.3)	0 (0)	1.0 (1.3)	0 (0)
QDEX3E	1.0	0	1.0	0
	2.1 (2.1)	0 (0)	2.1 (2.1)	0 (0)
	2.0 (2.0)	0 (0)	2.0 (2.0)	0 (0)
	2.1 (2.1)	0 (0)	2.1 (2.1)	0 (0)
QFEX4A	1.4	0.1	1.4	0.1
	2.8 (2.8)	0.3 (0.3)	2.8 (2.4)	0.2 (0.2)
	2.8 (2.6)	0.2 (0.2)	2.8 (2.8)	0.2 (0.2)
	2.8 (2.6)	0.2 (0.2)	2.9 (2.9)	0.2 (0.5)
QFEX4B	0	0	0	0
QFEX4C	0.4	0.4	0.4	0.4
	0.7 (0.7)	0.7 (0.7)	0.9 (0.4)	0.7 (0.3)
	0.7 (0.7)	0.7 (0.7)	0.5 (0.7)	0.4 (0.4)
	0.7 (0.7)	0.7 (0.7)	0.9 (0.4)	0.7 (0.5)
QFEX4D	0.3	0.3	0.3	0.3
	0.6 (0.6)	0.5 (0.5)	0.4 (0.6)	0.5 (0.2)
	0.6 (0.6)	0.5 (0.2)	0.6 (0.8)	0.5 (0.5)
	0.6 (0.9)	0.5 (0.5)	0.6 (0.6)	0.5 (0.5)
QFEX4E	0.1	25.4	0.1	25.4
	0.2 (0.2)	51.8 (51.8)	1.2 (0.2)	77.0 (76.8)
	0.2 (0.2)	50.8 (25.8)	0.2 (0.2)	49.8 (49.8)
	0.2 (0.2)	51.8 (51.8)	0.2 (0.2)	76.5 (38.4)

Table 3: Primary disrupted beam loss (kW) in the extraction collimators for the Nominal, Low Y-emittance and Low Power parameter options without and with IP *y*-offset in the case when the errors are NOT applied. Fast sweeping kickers are set to sweep the beam on *R* = 3 cm circle at dump.

Parameter Option	COLE	COLCD	COLW1	COLW2	COLW3
C11	0	0	0.16	0.08	0.93
C11, y-offset	0	0.08	3.85	3.34	8.92
C13	0	0.07	1.42	1.14	5.72
C13, y-offset	0	0	2.32	1.71	8.49
C14	0.10	0.97	10.27	8.15	21.46
C14, y-offset	0.34	11.53	63.66	38.60	61.34

3. MAGNET ERRORS AND CORRECTION

The real magnets will have field and alignment errors causing beam perturbation. In this paper, we consider that the field errors are applied to the detector solenoid, to the quadrupoles and dipoles and have a Gaussian width of 10^{-3} relative to the nominal setting and are applied to the elements in an uncorrelated manner. The misalignment is applied in the same way, where the Gaussian width of horizontal and vertical offset is $310\,\mu m$, and the roll error Gaussian width is $1.5\,mrad$. The longitudinal component of the solenoid field error $B_{s,Err}(s)$ is chosen to be +0.5% of the nominal field value $B_s(s)$; i.e. the total field is $B_{s,Err}(s) = 1.005 \cdot B_S(s)$. Bend field errors are simulated by thin lens kickers placed in the middle of the bend magnets. One random set of errors is used in this study. The rms field and alignment errors are summarized in Table 4.

Table 4: RMS values of field and alignment errors in the solenoid, quadrupoles and bend magnets.

ELEMENTS	$\Delta B/B$	Δx [μm]	$\Delta\theta_X$ [μrad]	Δy [μm]	$\Delta\theta_Y$ [μrad]	$\Delta\theta_S$ [μrad]
σ_{SOLEN}	0.005	50	500	50	500	0
σ_{QUAD}	0.001	100	0	50	0	350
σ_{BEND}	0.005	310	0	310	1500	1500

The disrupted beam losses on the normal conducting magnets should be limited to 100 W/m to avoid long-term radiation damage. The collimator losses can be much higher depending on the collimator design.

The errors applied to the extraction line result in a perturbation of the linear transport optics and distortion of the beam orbit. These distortions need to be corrected to give good polarimeter performance and ensure the disrupted beam power losses remain acceptable. The orbit correction at the secondary focus (Compton IP) and downstream of the polarimeter chicane can be done using the same set of kickers which are already used to correct the orbit generated by

the solenoid [8]. These kickers are labeled as VKEX1, VKEX2, HKEX1, HKEX2, VKPOL1, VKPOL2, HKPOL1, HKPOL2 and are located in the solenoid and polarimeter regions [8]. To ensure a good measurement at the polarimeter, the effects of focusing errors at the Compton IP will be compensated using two corrector coils on the extraction quadrupoles to maintain transfer matrix elements R_{12} and R_{34} close to zero between the IP and CIP.

Effects of various magnet errors on extracted beam trajectory are shown in Figures 3-8 (case a - before correction; case b - after correction), as calculated by MAD. Note that misalignment in these figures includes both the x/y magnet offsets and roll errors.

Effects of various errors on energy deposition in collimators for different beam parameter sets are presented in Tables 5-7, where the results after correction are shown in red colour. The effects of errors on energy deposition in quadrupoles for different beam parameter sets are presented in Table 2 shown earlier, where the column labeled "AFTER CORRECTIONS" is for the results after correction of the corresponding errors.

Tables 2 and 5-7 show that the effects of magnets errors do not significantly increase the beam power loss. The orbit correctors cancel the orbit perturbation of the beam core after the solenoid and in the polarimeter chicane, and maintain the correct beam core position and angle at CIP. However they also create residual dispersion which in some cases may somewhat increase losses in the beam low energy tail.

Tables 8-10 show the horizontal $< x >$ and vertical $< y >$ offsets of the beam core with $dp/p < 1\%$ at the Compton IP, the average spin projection P [8,14,15], and percentage of the beam particles within the laser spot κ at the Compton IP for different beam parameter sets (with and without y offset) when various types of errors are applied. The results after corrections are indicated in red colour. Here, the largest orbit offsets at Compton IP are caused by bend field and roll errors and quadrupole misalignment which are compensated by the orbit correctors. In most cases the correctors are able to correct the orbit at CIP to the original level without errors. They also maximize the percentage of particles within the laser spot. Note that the calculated $< y >$ offset at CIP has a small systematic negative component due to the design 2 cm vertical dispersion.

4. CONCLUSION

Effects of field and alignment errors in the ILC extraction line magnets were studied using one random set of errors for three ILC beam parameter options with and without beam offset at IP. It is shown that orbit perturbation of the beam core caused mostly by bend field and roll errors, quadrupole and solenoid misalignment and the incoming beam orbit can be corrected locally in the solenoid and polarimeter chicane regions using eight dipole correctors. The polarimeter correctors can also effectively adjust the orbit angle and position at the Compton IP for efficient polarization measurement. It is found that the studied errors do not significantly increase the extraction beam power loss even without orbit correction. The orbit correctors generate additional dispersion which in some cases may somewhat increase losses in the beam low energy tail. The calculated power losses in extraction magnets and collimators are within the acceptable range.
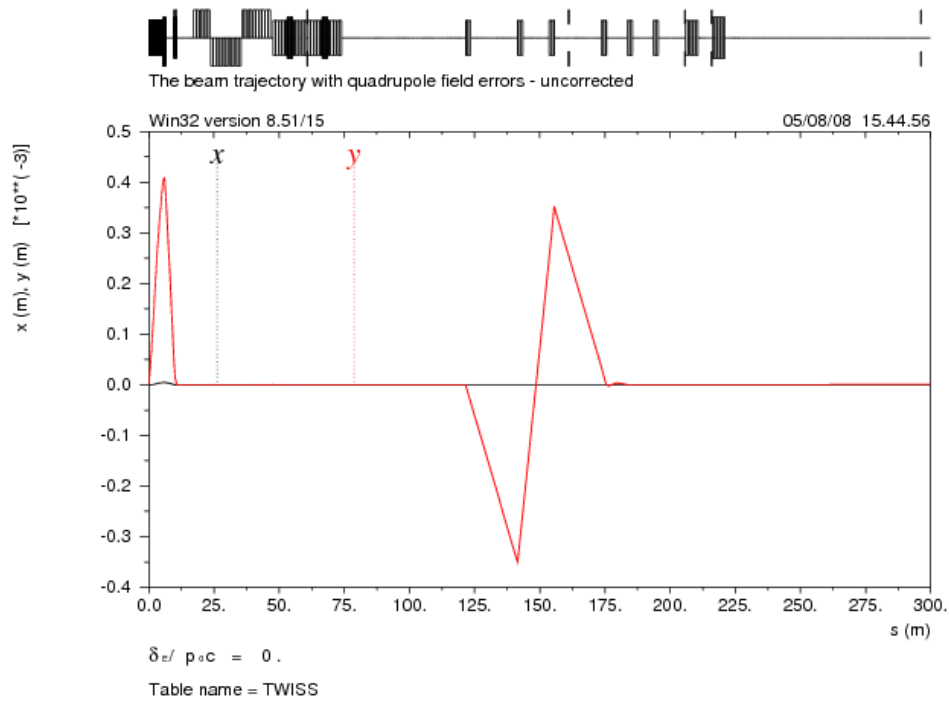
Figure 3a: Beam trajectory with quadrupole field errors before correction.
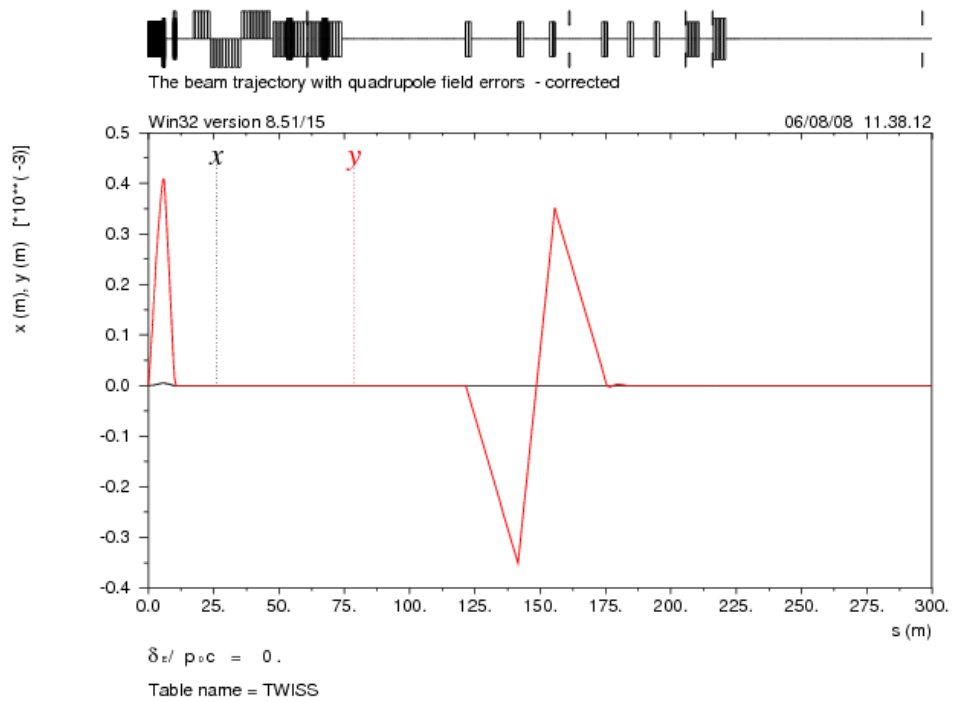
Figure 3b: Beam trajectory with quadrupole field errors after correction.

10
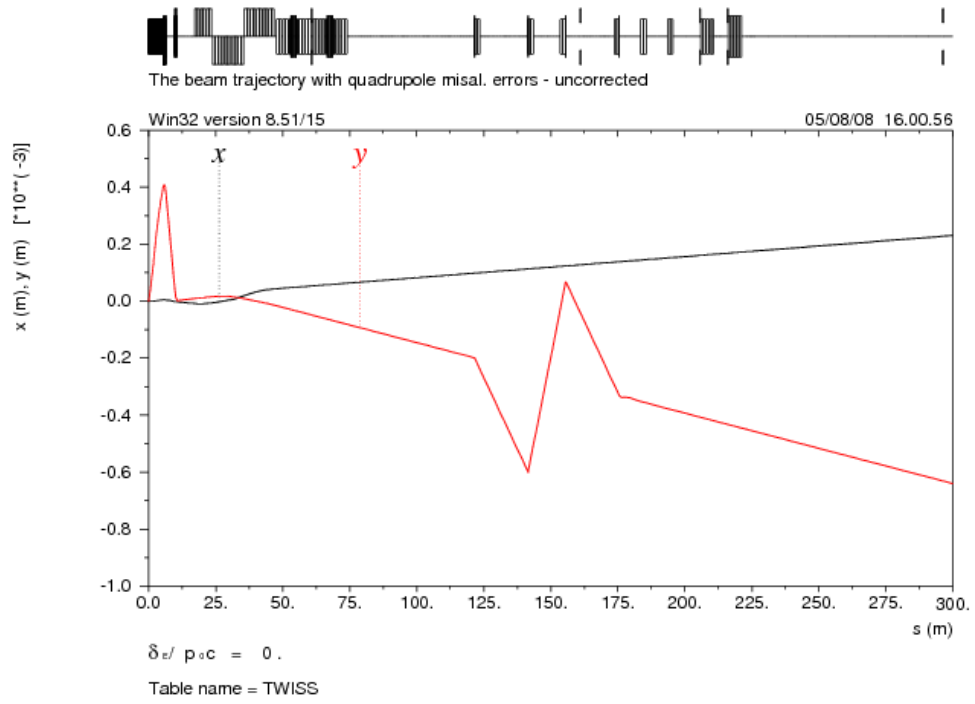
Figure 4a: Beam trajectory with quadrupole alignment errors before correction.
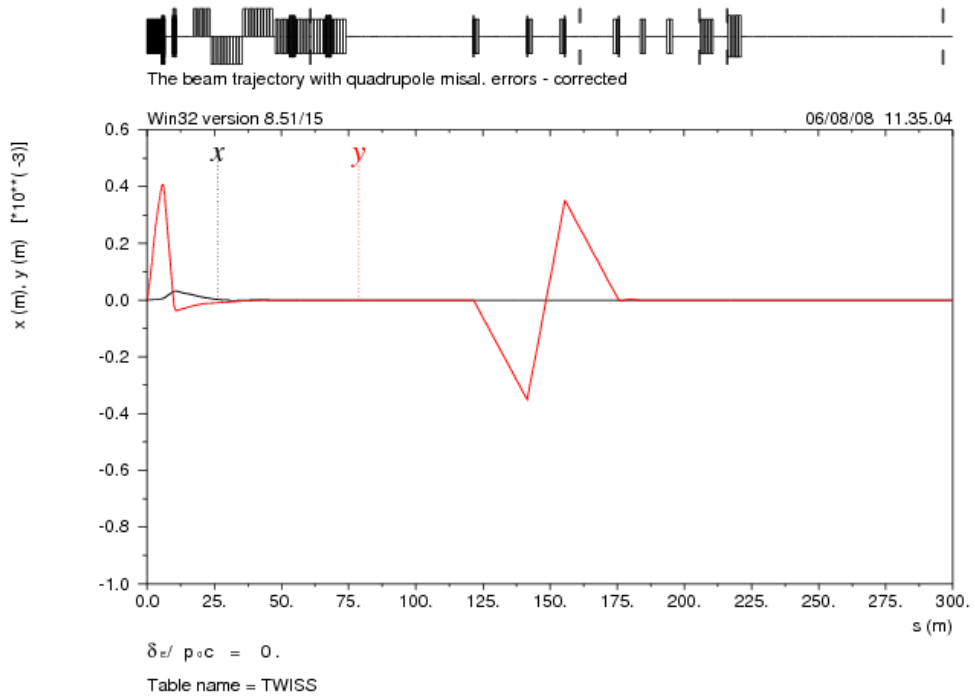
Figure 4b: Beam trajectory with quadrupole alignment errors after correction.

11
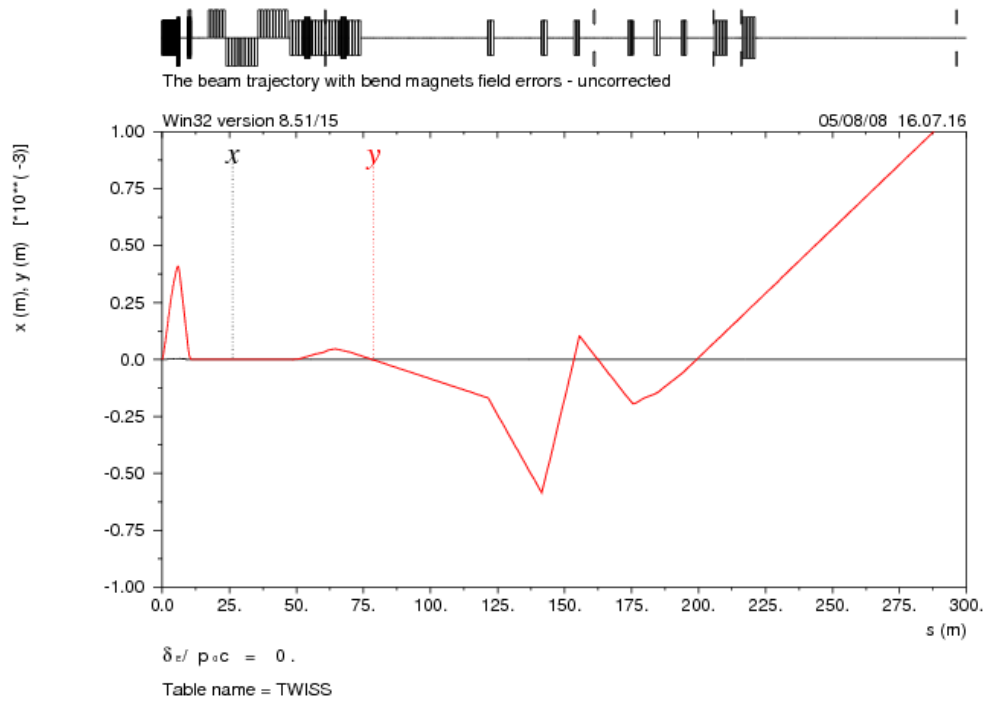
Figure 5a: Beam trajectory with bend magnet field errors before correction.
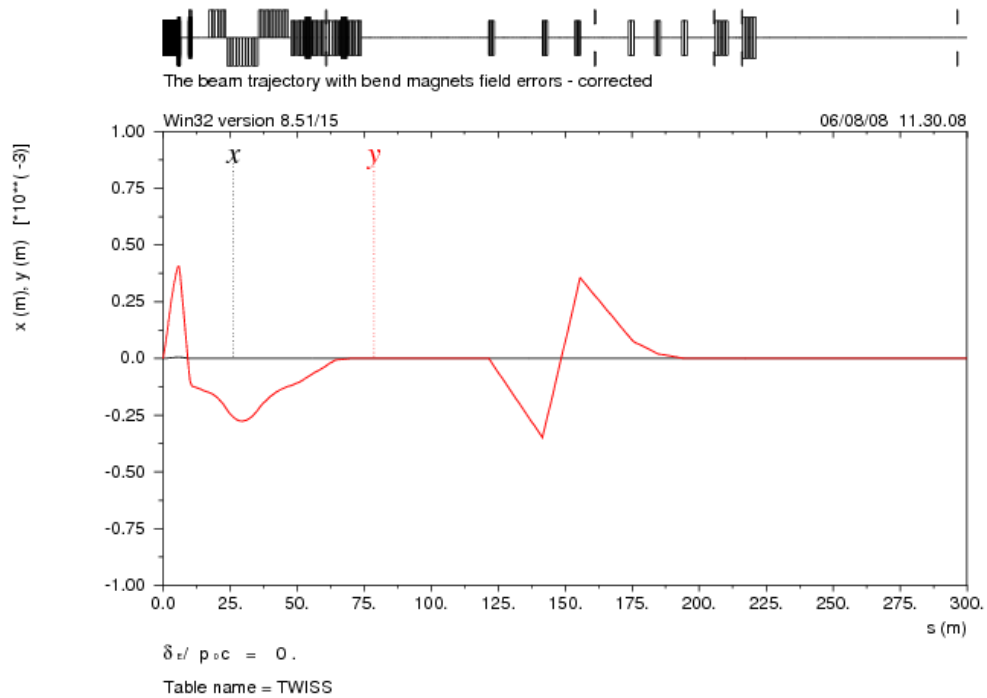
Figure 5b: Beam trajectory with bend magnet field errors after correction.

12
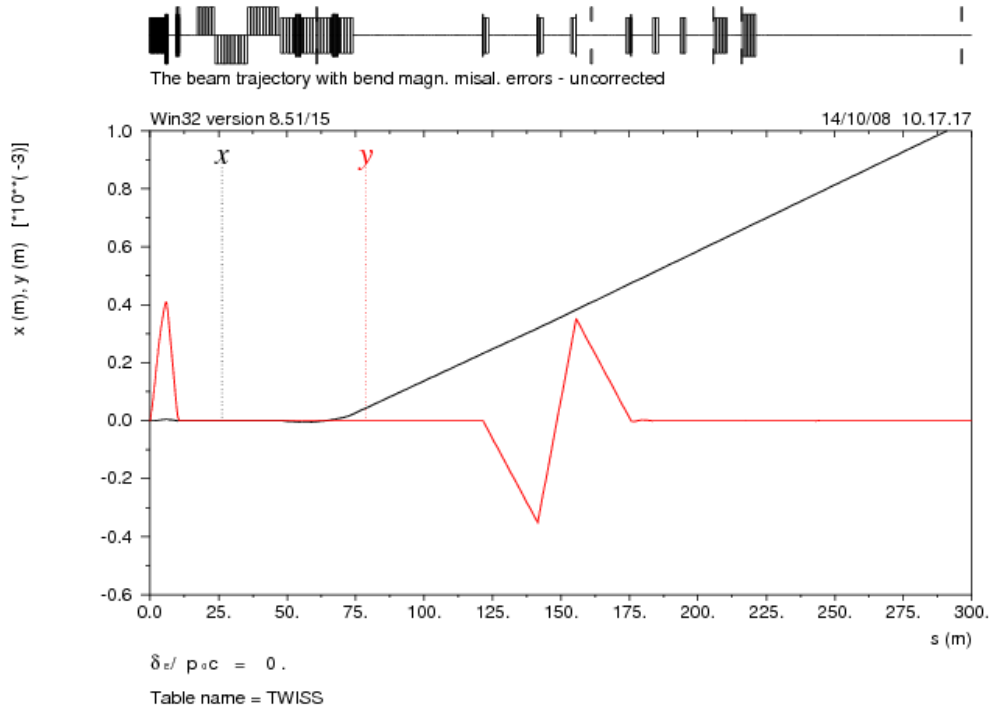
Figure 6a: Beam trajectory with bend magnet alignment errors before correction.
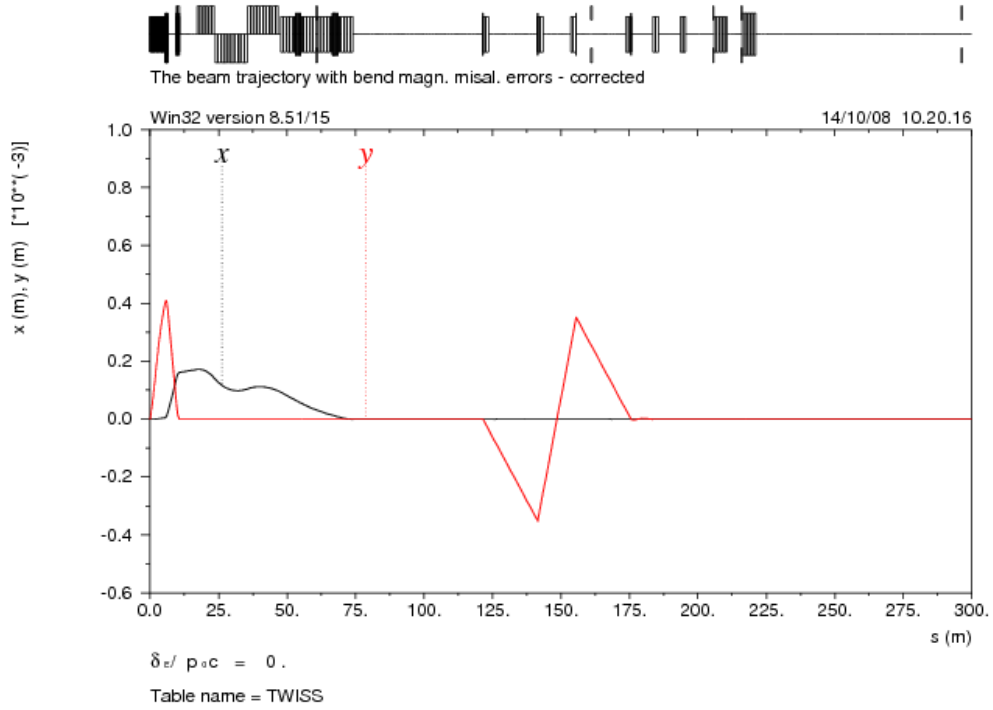
Figure 6b: Beam trajectory with bend magnet alignment errors after correction.

13
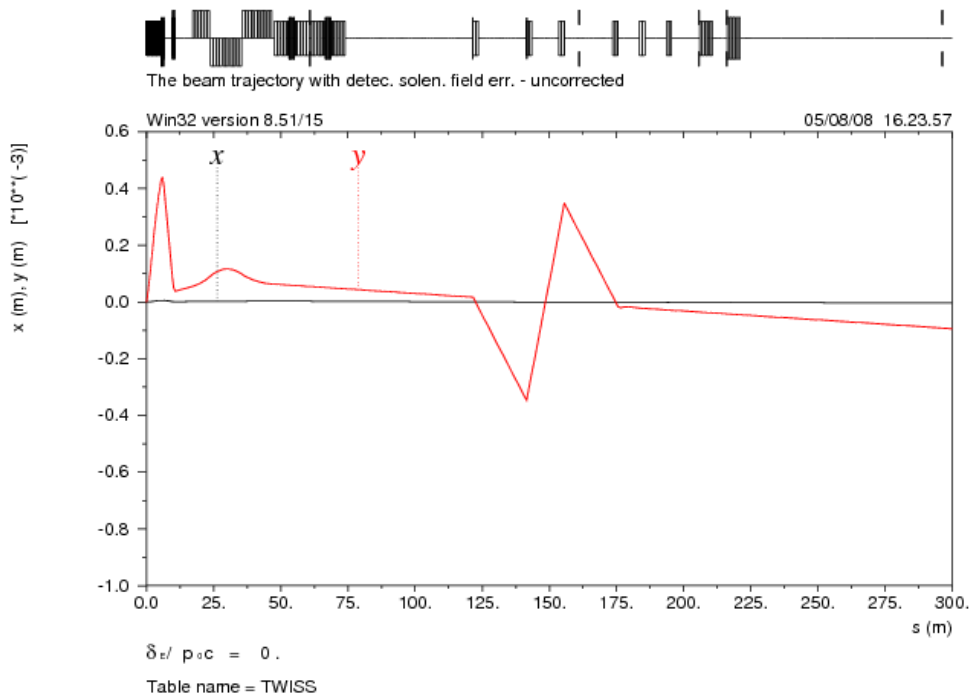
Figure 7a: Beam trajectory with detector solenoid field errors before correction.
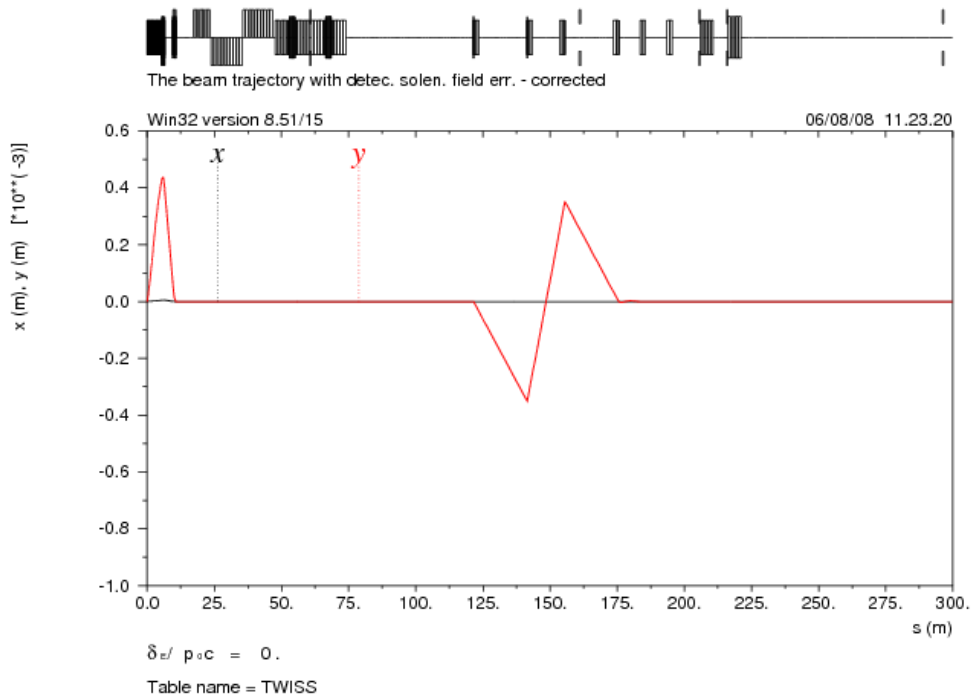
Figure 7b: Beam trajectory with detector solenoid field errors after correction.

14
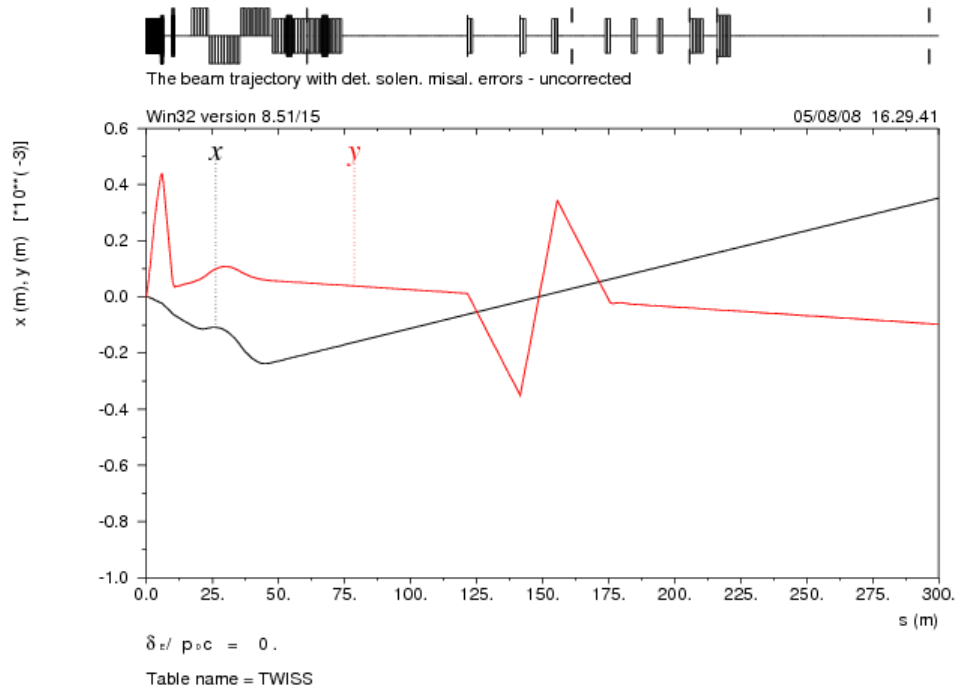
Figure 8a: Beam trajectory with detector solenoid alignment errors before correction.
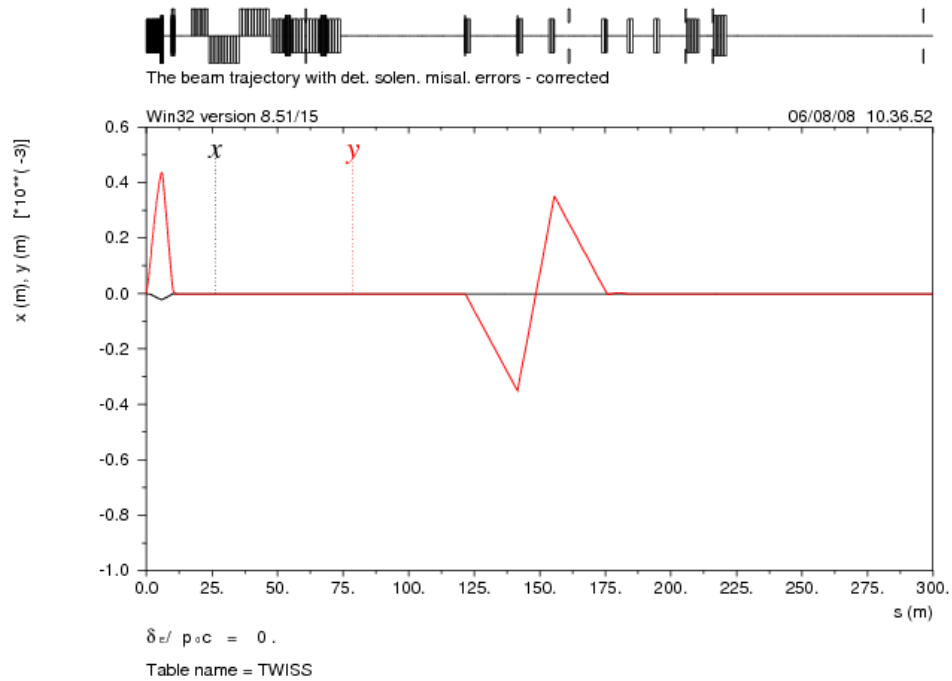
Figure 8b: Beam trajectory with detector solenoid alignment errors after correction.

15

Table 5: Primary disrupted beam loss (W) in the extraction collimators for the Nominal (C11) parameter option without and with IP *y*-offset for various types of errors. Red colour – after corrections. Fast sweeping kickers are set to sweep the beam on *R* = 3 cm circle at dump.

C11, $E = 500\,GeV$ center-of-mass					
Type off errors	**COLE**	**COLCD**	**COLW1**	**COLW2**	**COLW3**
NO Errors	0	0	160	79	926
Bend Field	0 1	0 0	160 160	79 79	1138 1137
Bend Misalignment	0 0	0 0	160 160	79 79	1093 1019
Quad Field	0 0	0 0	160 160	79 79	903 950
Quad Misalignment	0 0	0 0	77 77	142 162	852 832
Solenoid Field	0 1	0 0	160 239	79 93	926 1323
Solenoid Misalignment	0 0	0 0	160 239	79 93	977 1286

C11 y-offset, $E = 500\,GeV$ center-of-mass					
Type off errors	**COLE**	**COLCD**	**COLW1**	**COLW2**	**COLW3**
NO Errors	0	80	3854	3343	8920
Bend Field	3 7	80 317	3854 4881	3396 3594	9401 10221
Bend Misalignment	3 3	80 80	3763 3763	3412 3411	9039 8920
Quad Field	3 3	80 80	3765 3854	3344 3343	8840 8920
Quad Misalignment	3 3	80 80	3626 3626	2805 3170	7907 8247
Solenoid Field	3 4	80 234	3854 4284	3344 3409	8920 9323
Solenoid Misalignment	3 4	80 154	3660 3874	3352 3410	8871 9144

Table 6: Primary disrupted beam loss (W) in the extraction collimators for the Low Y-emittance (C13) parameter option without and with IP *y*-offset for various types of errors. Red colour – after corrections. Fast sweeping kickers are set to sweep the beam on *R* = 3 cm circle at dump.

C13, $E = 500\,GeV$ center-of-mass					
Type off errors	**COLE**	**COLCD**	**COLW1**	**COLW2**	**COLW3**
NO Errors	0	66	1421	1141	5716
Bend Field	4	66	1422	1142	5643
	7	66	1422	1216	5801
Bend Misalignment	4	66	1422	1065	5977
	4	66	1422	1142	5664
Quad Field	4	66	1422	1143	5692
	4	66	1421	1167	5615
Quad Misalignment	3	66	1339	1147	5613
	4	66	1339	1147	5504
Solenoid Field	4	66	1422	1142	5719
	6	66	1421	1167	5697
Solenoid Misalignment	4	66	1339	1127	5811
	6	66	1421	1065	6021

C13 y-offset, $E = 500\,GeV$ center-of-mass					
Type off errors	**COLE**	**COLCD**	**COLW1**	**COLW2**	**COLW3**
NO Errors	0	0	2322	1710	8494
Bend Field	0	0	2323	1765	8787
	0	0	2827	1851	9066
Bend Misalignment	0	0	2323	1792	8779
	0	0	2322	1684	8440
Quad Field	0	0	2322	1684	8490
	0	0	2323	1711	8475
Quad Misalignment	0	0	2221	1486	8365
	0	0	2221	1599	8652
Solenoid Field	0	0	2322	1684	8548
	0	0	2425	1826	8621
Solenoid Misalignment	0	0	2323	1549	8932
	0	0	2323	1711	8514

Table 7: Primary disrupted beam loss (W) in the extraction collimators for the Low Power (C14) parameter option without and with IP _y_-offset for various types of errors. Red colour – after corrections. Fast sweeping kickers are set to sweep the beam on _R_ = 3 cm circle at dump.

C14, $E = 500\,GeV$ center-of-mass					
Type off errors	**COLE**	**COLCD**	**COLW1**	**COLW2**	**COLW3**
NO Errors	104	966	10272	8150	21461
Bend Field	190	990	10580	8363	22535
	249	1377	11909	9535	23301
Bend Misalignment	190	990	10498	8362	22825
	190	990	10455	8446	21901
Quad Field	185	966	10144	8148	21475
	184	966	10594	8186	21616
Quad Misalignment	170	789	8881	8398	20986
	177	859	9309	8385	21311
Solenoid Field	190	990	10529	8316	21984
	179	1115	11113	8638	22801
Solenoid Misalignment	189	930	9815	8451	22128
	177	1112	10826	8316	23228

C14 y-offset, $E = 500\,GeV$ center-of-mass					
Type off errors	**COLE**	**COLCD**	**COLW1**	**COLW2**	**COLW3**
NO Errors	344	11528	63655	38603	61337
Bend Field	374	11700	65208	39599	63093
	528	16113	64196	35353	62744
Bend Misalignment	374	11816	65189	39830	63523
	374	11816	65347	39257	62372
Quad Field	364	11528	63451	38628	61064
	364	11415	63825	38834	61393
Quad Misalignment	334	9578	65250	40531	60778
	335	10360	64886	39596	61448
Solenoid Field	374	11776	65177	39676	62751
	370	13380	65054	37450	62802
Solenoid Misalignment	374	11306	65311	40794	63569
	370	12654	64761	39070	63695

Table 8: $< x >$ and $< y >$ offsets of the beam core with |Δp/p| < 1%, the average spin projection P, and the percentage of particles κ within laser spot at the Compton IP for Nominal (C11) beam parameter set (with and without y offset) when various types of magnet errors are applied. Red colour – after correction.

C11, $E = 500\,GeV$ center-of-mass				
Type off errors	$< x >$ $[\mu m]$	$< y >$ $[\mu m]$	$P\,[\%]$	κ
NO Errors	2.539	-48.226	99.82	46.3
Bend Field	2.539	-292.889	99.82	0.0
	2.519	-44.702	99.82	46.6
Bend Misalignment	354.333	-48.262	99.72	0.0
	-3.366	-48.244	99.82	46.2
Quad Field	2.445	-47.365	99.82	44.6
	2.676	-47.946	99.81	47.3
Quad Misalignment	191.327	-435.576	0.00	0.0
	72.437	-169.972	99.77	10.5
Solenoid Field	2.515	-48.314	99.82	46.3
	3.153	-46.840	99.82	46.4
Solenoid Misalignment	5.100	12.242	99.82	46.6
	2.744	17.821	99.82	46.5

C11 y-offset, $E = 500\,GeV$ center-of-mass				
Type off errors	$< x >$ $[\mu m]$	$< y >$ $[\mu m]$	$P\,[\%]$	κ
NO Errors	2.984	-51.474	99.82	33.1
Bend Field	2.984	-296.169	99.82	1.1
	3.318	-47.436	99.82	33.1
Bend Misalignment	354.867	-51.480	0.00	0.0
	-3.147	-52.076	99.82	33.1
Quad Field	2.834	-50.146	99.82	32.9
	3.065	-51.311	99.82	30.6
Quad Misalignment	191.810	-440.036	99.79	0.5
	72.735	-173.931	99.79	9.4
Solenoid Field	3.001	-51.525	99.82	33.1
	3.549	-49.311	99.82	33.1
Solenoid Misalignment	5.793	8.540	99.82	32.5
	3.245	14.390	99.82	32.1

Table 9: $<x>$ and $<y>$ offsets of the beam core with |Δp/p| < 1%, the average spin projection P , and the percentage of particles κ within laser spot at the Compton IP for Low Y-emittance (C13) beam parameter set (with and without y offset) when various types of magnet errors are applied. Red colour – after correction.

C13, $E = 500\,GeV$ center-of-mass				
Type off errors	$<x>$ $[\mu m]$	$<y>$ $[\mu m]$	$P\,[\%]$	κ
NO Errors	2.989	-58.097	99.69	32.9
Bend Field	2.989	-302.843	0.00	0.0
	3.363	-53.314	99.69	33.1
Bend Misalignment	354.946	-302.900	0.00	0.0
	-3.666	-57.890	99.69	32.9
Quad Field	3.521	-57.351	99.71	30.1
	2.833	-57.602	99.68	34.4
Quad Misalignment	191.761	-447.284	0.00	0.0
	72.477	-181.024	99.58	9.6
Solenoid Field	3.038	-58.190	99.69	32.9
	3.704	-56.221	99.69	32.9
Solenoid Misalignment	6.073	1.717	99.70	33.2
	3.112	7.763	99.70	33.1

C13 y-offset, $E = 500\,GeV$ center-of-mass				
Type off errors	$<x>$ $[\mu m]$	$<y>$ $[\mu m]$	$P\,[\%]$	κ
NO Errors	1.276	-59.175	99.76	27.3
Bend Field	1.276	-303.946	99.80	1.2
	0.910	-53.278	99.76	27.2
Bend Misalignment	353.267	-304.002	99.62	0.3
	-5.371	-59.592	99.76	27.2
Quad Field	0.782	-59.358	99.77	26.7
	1.059	-58.268	99.75	24.2
Quad Misalignment	189.565	-447.024	99.74	0.6
	70.819	-181.815	99.73	9.0
Solenoid Field	0.998	-59.311	99.76	27.3
	1.839	-57.252	99.76	27.3
Solenoid Misalignment	4.231	0.639	99.77	26.7
	1.956	6.875	99.77	26.4

Table 10: $<x>$ and $<y>$ offsets of the beam core with |Δp/p| < 1%, the average spin projection P, and the percentage of particles κ within laser spot at the Compton IP for Low Power (C14) beam parameter set (with and without y offset) when various types of magnet errors are applied. Red colour – after correction.

C14, $E = 500\,GeV$ center-of-mass				
Type off errors	$<x>$ $[\mu m]$	$<y>$ $[\mu m]$	$P\,[\%]$	κ
NO Errors	2.372	-54.113	99.17	72.7
Bend Field	2.372	-298.810	99.13	
	2.248	-50.035	99.15	72.6
Bend Misalignment	354.257	-54.118	99.13	
	-4.049	-54.029	99.17	72.8
Quad Field	2.866	-52.947	99.17	74.6
	2.418	-54.027	99.17	71.7
Quad Misalignment	191.061	-442.516	99.15	
	72.994	-176.537	99.17	91.2
Solenoid Field	2.379	-54.187	99.17	72.7
	3.177	-52.093	99.16	72.7
Solenoid Misalignment	4.717	5.979	99.17	72.6
	2.815	12.108	99.17	72.8

C14 y-offset, $E = 500\,GeV$ center-of-mass				
Type off errors	$<x>$ $[\mu m]$	$<y>$ $[\mu m]$	$P\,[\%]$	κ
NO Errors	-1.216	-59.196	98.34	83.0
Bend Field	-0.570	-304.386	98.44	80.5
	-0.842	-55.118	98.28	83.0
Bend Misalignment	350.767	-59.201	98.44	80.0
	-7.578	-58.938	98.35	83.0
Quad Field	-1.311	-58.047	98.36	84.2
	-0.341	-59.236	98.36	85.4
Quad Misalignment	187.896	-447.487	98.48	87.2
	68.832	-181.067	98.44	93.7
Solenoid Field	-1.044	-59.499	98.35	83.0
	-0.234	-57.188	98.32	83.0
Solenoid Misalignment	2.467	0.186	98.36	83.3
	-0.059	7.163	98.34	83.5

5. ACKNOWLEDGEMENT

References

[1]   J. Brau (Ed.) et al., "ILC Reference Design Report: ILC Global Design Effort and World Wide Study", FERMILAB-APC (2007).

[2]   MAD-8 program, http://mad.web.cern.ch/mad/mad8web/mad8.html .

[3]   DIMAD program, http://www-project.slac.stanford.edu/lc/local/AccelPhysics/dimad.pdf .

[4]   Y. Nosochkov et al., "14 mrad Extraction Line Optics for Push-Pull", SLAC-PUB-12856, LCWS-2007-MDI13 (2007).

[5]   B. Parker et al., "The Superconducting Magnets of the ILC Beam Delivery System", PAC07-THPMS091, SLAC-PUB-12832 (2007).

[6]   SiD Design Study, http://silicondetector.org/display/SiD/home .

[7]   T. Behnke (Ed.) et al., "ILC Reference Design Report Volume 4 – Detectors", FERMILAB-APC (2007).

[8]   D. Toprek, Y. Nosochkov, "Evaluation and Compensation of Detector Solenoid Effects on Disrupted Beam in the ILC 14 mrad Extraction Line", SLAC-PUB-13492 (2008).

[9]   K. Moffeit et al., "Proposal to Modify the Polarimeter Chicane in the ILC 14 mrad Extraction Line", SLAC-PUB-12425, IPBI-TN-2007-1 (2007).

[10]   D. Schulte, "Study of Electromagnetic and Hadronic Background in the Interaction Region of the TESLA Collider", PhD. Thesis, TESLA-97-08 (1996).

[11]   T. Raubenheimer, "Suggested ILC Beam Parameter Range, Rev. 2/28/05", http://www-project.slac.stanford.edu/ilc/acceldev/beampar/Suggested%20ILC%20Beam%20Parameter%20Space.pdf (2005).

[12]   A. Seryi, http://www.slac.stanford.edu/~seryi/ILC_new_gp_files/ (2005).

[13]   Y. Nosochkov, T.O. Raubenheimer, K.A. Thompson, "NLC beam properties and extraction line performance with beam offset at IP", SLAC-PUB-8872, PAC-2001-FPAH065 (2001).

[14]   M. Woods et al., "Luminosity, energy and polarization studies for the linear collider: Comparing e+ e- and e-e- for NLC and TESLA", SLAC-PUB-10353, IPBI-TN-2004-1 (2004).

[15]   P.C. Rowson, M. Woods, "Experimental issues for precision electroweak physics at a high luminosity Z factory", SLAC-PUB-8745 (2000).